The fundamental difference between cleavage and hydrogen-assisted quasi-cleavage in ferritic materials revealed by multiscale quantitative fractographic and side surface characterization

Evgeniy Merson[1*], Pavel Myagkikh[1], Vitaliy Poluyanov[1], Maxim Dorogov[2], Dmitri Merson[1], Alexei Vinogradov[3]

[1]*Institute of Advanced Technologies, Togliatti State University, Belorusskaya str. 14, Togliatti 445667, Russian Federation*

[2]*International Research Center of Functional Materials and Devices of Optoelectronics, ITMO University, Kronverksky Pr. 49, St. Petersburg, 197101, Russian Federation*

[3]*Department of Mechanical and Industrial Engineering, Norwegian University of Science and Technology – NTNU, N-7491 Trondheim, Norway*

**Email: mersoned@gmail.com*

Abstract

The fracture surfaces and cracks in technically pure iron, Fe-2.5% Si alloy and low-carbon steel grade S235JR produced by quasi-cleavage (QC) hydrogen-assisted cracking (HAC) as well as by true cleavage (TC) were studied and compared on different scales through the quantitative and qualitative fractographic and side surface examinations. The mixed type QC/TC fracture surfaces were obtained using two-step mechanical testing methods involving the tension of the through-notched specimens under in-situ hydrogen charging followed by rapid fracture in liquid nitrogen. The side surface and fractographic examinations, including the quantitative facets analysis, were conducted using scanning electron microscopy (SEM), confocal laser scanning microscopy (CLSM) and electron-backscattering diffraction (EBSD) technique. It is established, that the QC and TC fracture surfaces demonstrate fundamentally different morphological and topological features in all materials investigated. It is found that, depending on the material, the average angle of misorientation (AM) between the QC facets is 1.5-2 times lower than that of the TC facets. Thus, it is concluded that the crystallographic orientation of QC facets is generally different from TC. Owing to this feature, the path of the QC HAC through the microstructure of all investigated materials is featured by the remarkably lower spatial out-of-plane deviation on the scale equal to or larger than a few facets. Conversely, on the scale of an individual facet, the path of QC HAC deviates to a greater extent than that of the TC crack. This fundamental difference between QC HAC and TC cracking is found to be not significantly influenced by the chemical composition of the ferritic alloys.

Keywords: quasi-cleavage, hydrogen-assisted cracking, confocal laser scanning microscopy, hydrogen embrittlement, iron, fractography

1. Introduction

Most structural metals and alloys interacting with hydrogen are susceptible to hydrogen embrittlement (HE) – the extremely dangerous phenomenon causing the degradation of mechanical properties, the transition of the fracture mode from ductile to brittle and resulting in sudden failures of metallic components. Over the years, the greatest attention has been paid traditionally to HE of steels due to their abundance in structural applications in oil and gas, aerospace and automobile industries where the risk of HE is exceptionally high. The additional surge of interest towards the development of HE-resistant steels was ignited recently by the burgeoning activity and remarkable progress in the field of green energy centred on the wide use of hydrogen. Due to the excellent properties-to-cost ratio, low-carbon steels are considered as the promising candidates to be used in the hydrogen gas transportation and storage infrastructure. However, in spite of huge efforts, the scientifically-based approaches for the microstructural design of HE-resistant steels and for the prediction of their service life in hydrogen-bearing environments still face substantial challenges because of insufficient understanding of the underlying mechanisms responsible for HE. Perhaps, the most long-lasting but still unfinished dispute over the nature of the HE phenomenon is whether hydrogen promotes true brittle cracking or it is just a "masked" ductile fracture process preceded by hydrogen-assisted micro-void nucleation and coalescence (MVC). The apparent controversy between the two viewpoints stems from the complexity of fractographic features and the specifics of the crack path in the microstructures "poisoned" by hydrogen.

The common mode of brittle fracture occurring in pure iron, low-carbon steels and other bcc iron-based alloys is known as true cleavage (TC) [1,2]. This fracture mode dominates when dislocation slip is restricted, for example, due to low temperature, and the stress required for plastic deformation to proceed becomes comparable to or exceeds the cohesive interatomic strength. TC occurs by unstable transgranular crack extension due to the very fast sequential breaking of interatomic bonds along the well-defined low-index crystallographic planes. In bcc iron and steels, these planes are primarily of the {100} family [1–5], though the minor contribution from other low-index planes such as {110} and {112} is also possible [2,3]. The fracture surface produced in this way in polycrystals is composed of TC facets – the misoriented planar regions decorated by fan-like river patterns. Although the TC facets are occasionally found in hydrogen embrittled steels and iron [6,7], they are relatively uncommon, while the

primary fracture mode for the ferritic materials affected by hydrogen is quasi-cleavage (QC) [8–11]. This kind of fracture surface can be produced by hydrogen-induced cracking (HIC) [12–14], hydrogen-assisted cracking (HAC) [15,16], and hydrogen-assisted fatigue crack growth (HAFCG) [17,18]. All these three phenomena are driven by the cooperative action of diffusible atomic hydrogen and stress, which can be either internal or external. HIC is associated with the internal stress caused by the high pressure of molecular hydrogen precipitating within the discontinuities in the microstructure. The external stress applied to the hydrogen charged material by static or cyclic mechanical loading is responsible for HAC and HAFCG, respectively. The QC morphology produced in all these specific conditions exhibits similar plasticity-related markings seen as nano-dimples, tear ridges, slip-traces and striations [19], which are uncommon for TC. The "ductile-like" appearance of QC was considered as the evidence for the significant, or even decisive, role of plasticity in the mechanism producing the specific QC fracture relief [8,9,14,20,21]. The opposite viewpoint has been, however, advanced by many authors [13,15,16,18] that the QC fracture surface is formed by the TC mechanism, while plastic deformation serves as a concomitant accommodative process affecting the morphology of the fracture surface. Both opinions are reflected in several distinct HE models, including hydrogen enhanced decohesion (HEDE), hydrogen enhanced localized plasticity (HELP), adsorption induced dislocation emission (AIDE) and hydrogen enhanced strain-induced vacancy formation (HESIV). Besides, various hybrids of these models were proposed in an attempt to reconcile the antagonistic concepts and to provide a united explanation for the abundance of experimental data accumulated up to date in the field of HE. Despite the numerous experimental observations, calculations and numerical simulations supporting the proposed models to a smaller or greater extent, none of them is accepted in general as yet. A comprehensive overview of the aforementioned theories and mechanisms can be found elsewhere [22–26].

To clarify the nature of QC, the crystallographic orientation of cracks and fracture surfaces, as well as the relation between the crack path and microstructure, have been extensively studied in hydrogen-charged pure iron, Fe-Si alloys and low-carbon steels. Through the investigation of etch pits arrays on metallographic cross-sections, Tetelman and Robertson [27] and Gell and Robertson [28], for the first time, showed that the hydrogen-induced cracks (HICs) in Fe-3%Si single crystals align with {100} crystallographic planes. Using the two-surface trace analysis and electron-backscattering diffraction techniques (EBSD), Nakasato and Bernstein [14] and Marrow et al. [13] confirmed the {100} orientation of HICs in Fe-3%Si single crystals. The {100} crystallographic orientation was established by several authors for QC

fracture surfaces produced by HAC in the notched Fe-2.6% Si [21,29], Fe-3%Si [16] and Fe-3.2%Si [30] single crystals subjected to tensile testing along their [001] direction. Takahashi et al. [31] demonstrated that when both the notch and (011) plane are perpendicular to the tensile axis, the HAFCG in Fe-3.2%Si single-crystal occurs along the {110} planes. The authors stated that such HAFCG is not assisted by hydrogen-induced cleavage or the MVC process. Vehoff and Rothe [29] have also mentioned that when the tensile axis was aligned with [011] direction of the Fe-2.6% Si single-crystal, the macro-plane of fracture surface had the {110} orientation; however, at the micro-scale, the HAC occurred along the {100} planes. Since the {100} orientation is a known attribute of TC planes, most of the researchers agreed that HIC and HAC in Fe-Si alloys are governed by the cleavage-like mechanism [13,16,27–29]. As opposed to this, Lynch suggested that {100} crack growth can be alternatively explained by the AIDE scheme implying the key role of plasticity in the formation of the QC surface [21]. Although the {100} orientation was found to be characteristic of QC in Fe-Si single crystals, the less transparent results were obtained for pure iron and low-carbon steels. Nakasato and Bernstein [14] showed that the transition from cleavage plane to slip plane HIC occurs in Fe-Si single and bi-crystals with the Si content of 0.7%. In pure iron the HICs were aligned with {110} and {112} planes. The fracture surface of these cracks was featured by striations and tear ridges, which are typical of the QC morphology. Alike in Fe-Si alloys at room temperature and the [001] tensile axis, QC HAC in the notched single crystals of pure iron commonly occurs along the {100} planes [6,32,33]. However, at lower temperatures and other crystallographic orientations with respect to the tensile axis, as well as in the absence of the notch, the {100}, {110}, {112}, as well as some uncertain orientations of the QC fracture surface, have been reported [6,7,32,33]. The contradictory results have also been obtained for polycrystalline materials. With the aid of the one-surface trace analysis, EBSD and transmission electron microscopy (TEM), Birenis et al. [15] found that HAC in polycrystalline iron occurs primarily along the {100} planes when tensile testing is performed at 0.7 MPa hydrogen gas pressure, whereas {112}, {110} and {100} segments of the crack path were observed at higher hydrogen pressure. With the use of the same methods, it was demonstrated in several publications [17,18,34] that HAFCG occurs mainly along {100} planes in pure polycrystalline iron and ferrite-pearlite steel. In contrast, Takahashi et al. [35] established that the orientation of the QC facets produced by HAFCG in low-carbon steel was out of the {100} planes. The prevalence of the {110} orientation [36] or coexistence of {100}, {110} and non-specific index orientations [37] of QC facets was observed with the use of the two-surface trace analysis and EBSD technique in low-carbon steels fractured due to HAC.

The corollary from this overview is that despite the numerous attempts and variety of utilized experimental approaches, ambiguous results have been accumulated in regard to the QC HAC path and its relation to the underlying crystallography up to date. In particular, the question – whether the crystallography of QC matches to that of TC or not remains open as yet. Although the {100} orientation is the most frequently reported one, especially for the notched single crystals, the {110} and {112} QC facets are often observed in single- and polycrystalline ferritic materials. The fact of the existence of QC facets with the crystallographic orientation other than {100} cannot rule out the suggestion that QC HAC is governed by the cleavage-like mechanism since the TC facets in steels can also be occasionally formed along the {110} and {112} planes [2,3]. The presence of {100} facets and cracks does not prove this suggestion either. Apparently, reliable information regarding the statistical significance of the facets with different orientations corresponding to both fracture modes is strongly required to clarify the issue. However, there is an obvious deficiency of statistically representative data on the orientation of QC and TC facets in polycrystalline ferritic materials. For this reason, it is unknown whether the discrepancy of the literature data on the crystallographic orientation of QC is due to the intrinsic features of each material and specific HE conditions (e.g., HIC, HAC and HAFCG) or it is simply attributed to the insufficient data. For example, as was shown above, different crystallographic features are reported for QC in polycrystalline low-carbon steels and pure iron subjected to HAC and HAFCG. Besides, the effect of Si on the crystallographic orientation of HIC, which is shown in [14], challenges the relevance of the substantial part of available data obtained on the model Fe-Si alloys. Thus, the crystallography of QC HAC in polycrystalline Fe-Si alloys is of particular interest.

The precise and reliable determination of the crystallographic orientation of cracks and fracture surfaces in metallic materials commonly includes two independent operations, namely (1) the identification of the spatial orientation of the crack or the fracture plane in crystal coordinates and (2) the identification of the crystallographic orientation of the crystal itself. Both tasks can be implemented in a few ways. The most common approach to reveal the spatial orientation of the crack or the fracture surface is the two-surface trace analysis, which is based on the examination of two parallel or intersecting cross-sections of the crystal containing the traces of the same crack or the fracture surface. In turn, the crystallographic orientation of the crystal containing the crack can be conducted by the EBSD technique, the X-ray diffraction method, TEM or by the analysis of etch pits arrays. All these methods have been applied in HE studies discussed above. However, the acquisition of a representative dataset with these techniques is a nontrivial, laborious and complex task. Thus, the conclusions are usually inferred

from the results obtained from very limited data - a few single crystals or a couple of dozens of cracks and facets, at best. This approach can be critically misleading for polycrystalline materials where a considerably greater data sample is necessary for the conclusive understanding of the overall crystallographic orientation of fracture surfaces. To overcome these limitations, we proposed a technique for the facets misorientation analysis based on quantitative confocal laser scanning microscopy (CLSM) as described in detail in [38–41]. Although this technique does not allow for the determination of the exact crystallographic orientation of specific facets, it is capable of providing sufficiently large datasets for the statistical analysis of their spatial orientation and topographic features. This enables arriving at quantitative criteria for the reliable distinguishing between different fracture modes and different kinds of facets. The underlying mechanisms can be revealed and justified on this basis. For instance, it was shown that angles of misorientation between adjacent QC facets in hydrogen embrittled low-carbon steel have the twice lower average value and a fundamentally different distribution compared to those of TC facets in the same steel fractured in liquid nitrogen [41]. However, since the specimen with QC facets was more heavily deformed than the one tested at low temperature, the difference between the facets could result from the different extent of plastic deformation. To minimise the influence of plastic deformation, tensile testing under in-situ hydrogen charging followed by final fracture in liquid nitrogen was proposed in our recent publications [38,42] as a proof-of-concept to obtain the fracture surface containing both QC and TC facets. In the present investigation, we utilise the same method for the quantitative fractographic comparison between the hydrogen-related QC and TC facets in ferritic materials, including pure iron, Fe-Si alloy and low-carbon steel. The quantitative CLSM analysis was supplemented by side surface examinations providing insight into the features of the crack path produced by different fracture modes.

2. Experimental

2.1. Materials and specimens

The flat rectangular through-notched specimens, the geometry of which is represented in Fig. 1, were cut with an electric discharge machine along the rolling direction from the hot-rolled plates of commercial technically pure iron, Fe-2.5%Si alloy and low-carbon steel grade S235JR. For simplicity, these materials are referred to as iron, Fe-Si alloy and steel, respectively, throughout the rest of the paper. Chemical compositions of the materials used are listed in Table 1. The thickness of the specimens was 2 mm for Fe-Si and iron, and 2.5 mm for steel. The specimens were grinded down to 2500 grit emery paper and then polished by 3, 1 and 0.25 μm diamond suspensions and ultrasonic etched in 0.5 % HNO_3 for 20-30 s. The specimens of steel and iron were annealed in vacuum at 950 °C for 1 h followed by furnace cooling.

Table 1 – Chemical compositions of the materials used (wt. %)

Material	C	Si	Mn	P	S	Cr	Ni	Al	Cu	Fe
Pure iron	0.032	0.05	0.335	0.011	0.005	0.019	0.018	0.002	0.034	Balance
Fe-2.5%Si	<0.001	2.51	0.014	0.005	0.005	0.012	0.046	0.005	0.018	
S235JR	0.129	0.02	0.420	0.019	0.015	0.050	0.007	0.028	0.067	

2.2. Mechanical testing and hydrogen charging

To obtain the mixed-mode fracture surface composed of QC and TC regions with distinct boundary between them, the two-step mechanical testing has been implemented in the present study, as illustrated in Fig. 1. The first step loading under in-situ hydrogen charging conditions was performed in the same way as that described in [43]. This method was proven effective for producing the pure QC fracture surface in S235JR steel. The uniaxial tensile testing at this step was conducted using a screw-driven frame AG-X plus (Shimadzu) at 0.1 mm/min cross-head velocity at ambient laboratory temperature of 24±1 °C. For the in-situ hydrogen charging, the polyethylene electrochemical cell was mounted on the middle part of the specimen, such that the 5.4 cm^2 area of the specimen's surface around the notch was constantly exposed to the electrolyte during the testing. The platinum spiral wire surrounding the specimen was used as an anode. The tensile testing and hydrogen charging at 5 mA/cm^2 were simultaneously turned on as soon as the electrolytic cell was filled up with the 5% H_2SO_4 + 1.5 g/l thiourea solution. Thus, no pre-charging occurred before testing. It was shown in [43] that such a combination of hydrogen charging and mechanical testing conditions provides stable QC HAC but does not produce any notable hydrogen-induced damage such as hydrogen-induced cracks and/or blisters. The specimens were stretched up to a pre-set strain, at which the crack growing from the notch reached of 1 - 1.7 mm in length. The required strain value was found experimentally by testing a few specimens of each material. As soon as the needed crack length was reached, the test was interrupted. The specimen was unloaded, extracted from the electrolytic cell, rapidly and carefully cleaned with ethanol in ultrasonic bath and dried with compressed air. After that, the side surface of the specimen was examined by scanning electron microscopy (SEM) to document and to characterise the state of the main and secondary cracks associated with the HAC mechanism. Next to this intermediate side surface examination, the specimen was subjected to the second-step tensile testing, which was performed in the liquid nitrogen bath at 1 mm/min

cross-head velocity up to the complete fracture of the specimen. The method described above allowed obtaining the fracture surfaces composed of pure QC morphology followed by the region consisting of TC facets only, since the influence of hydrogen during the testing in liquid nitrogen can be neglected.

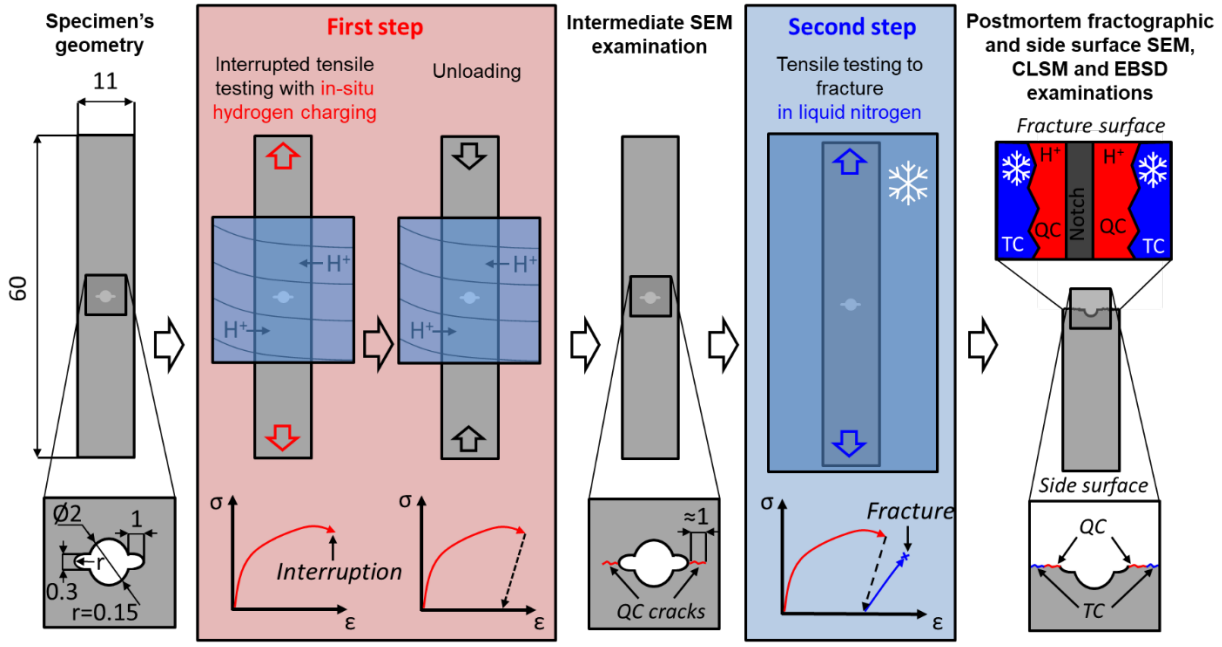

Fig. 1 – The schematic illustration of the two-step mechanical testing procedure supplemented by intermediate and post-mortem SEM examinations.

2.3. Fractographic and side surface observations

The fracture and side surfaces of the tested specimens were qualitatively investigated using SEM JCM-6000 (JEOL) and CLSM Lext OLS4000 (Olympus). The side surface study by EBSD method was conducted using the Tescan Amber SEM equipped with Oxford Instruments EBSD facilities and proprietary software.

The quantitative fractographic analysis was performed using the topographic data acquired and processed by CLSM. The fracture surfaces were scanned by the MPlanApoN50xLEXT objective lens featuring by 1000x magnification and by the view field of 256×256 μm^2 area. The step height of 0.3 μm was used for scanning along the vertical Z-axis. Each scan conducted in this way produces the array of colour, light intensity and height values enabling the 3D reconstruction of the surface topology as well as the creation of conventional colour- and grey-

scale 2D images. At least six scans were obtained for each kind of fracture mode (QC and TC) in each material investigated. All the images were de-noised with the "pre-measurement' digital filter provided by the original microscope's software. The root mean square (Sq) areal roughness has been evaluated for all the obtained height arrays in accordance with the ISO 25178 guidance.

The quantitative facets analysis was performed with the use of the homemade software providing an evaluation of the inclination angles of facets to each other. The workflow of the analysis is summarised as follows. Both the 2D CLSM image and the corresponding height matrix are fed to the software. The operator manually outlines the facets on the 2D image. The algorithm finds the region of the heights array associated with the outlined facet and approximates it with the plane. Finally, using the coefficients of the plane equation, the angles of misorientation (AM) between the adjacent facets are calculated. Besides, the unevenness of the facets is quantitatively assessed by the mean standard deviation of approximation (D), which serves as a gross measure of the quality of fit and indicates the deviation of the facet's surface relief from the best approximating plane. In the present study, at least 500 facets of each kind (QC or TC) have been analysed to calculate the average values of the aforementioned parameters for each material. To calculate the average value of the angle of misorientation for the specific types of facets, of 800-1000 angles between adjacent facets were acquired. Using the mean values obtained for every 256×256 μm^2 region, the average values and the corresponding mean standard deviations of all investigated parameters were calculated for the specific kind of fracture surface in all the materials. Within the ranges of the calculated mean standard deviations, the technique used showed good reliability and reproducibility for distinguishing between different kinds of fracture morphologies. For further methodological details of the procedure, a reader is referred to refs. [39–41].

3. Results

3.1. Microstructure

The metallographic analysis showed that the microstructure of all investigated materials is composed of relatively large equiaxed ferritic grains with an average diameter of 36, 52 and 79 μm for steel, Fe-Si alloy and iron, respectively, Fig. 2. Besides, all tested materials contain numerous non-metallic inclusions. The microstructure of steel is featured by pearlitic grains, Fig. 2c. According to the EBSD data provided in Fig. 2d-i, the angular misorientation of grains in all the materials is fairly close to random, which is represented by the theoretical Mackenzie's distribution. Albeit, it is worth noting that, on average, the grains of Fe-Si alloy possess slightly

lower misorientation than in two other materials, as is indicated by the shift of the histogram in Fig. 2h towards the left with respect to the random distribution.

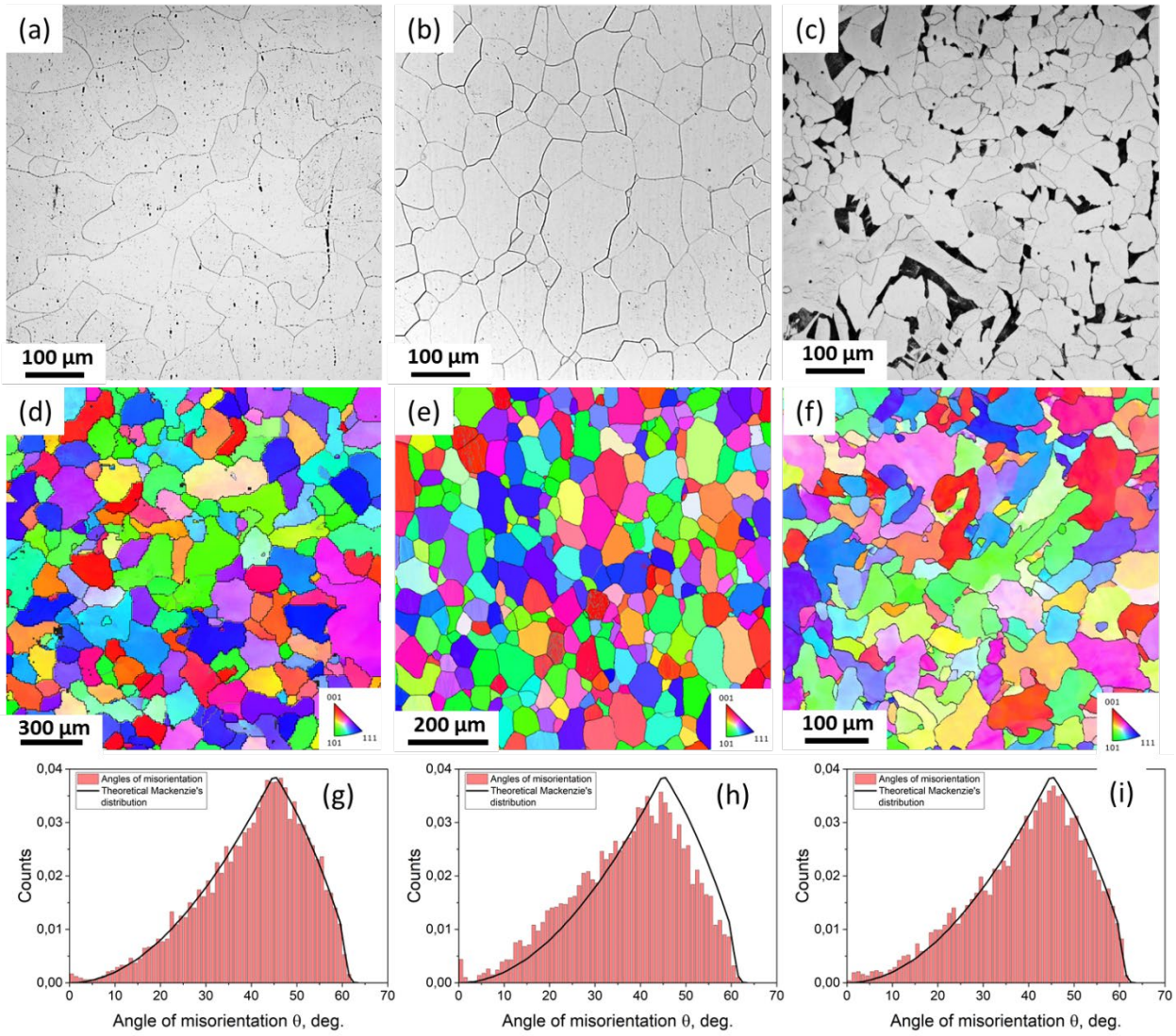

Fig. 2 – Microstructure of technically pure iron – (a, d, g), Fe-2.5%Si alloy – (b, e, h) and low-carbon steel S235JR – (c, f, i) characterised by the CLSM metallographic images – (a-c), EBSD inverse pole figure (IPF) maps – (d-f) and distribution histograms of angles of misorientation between grains superimposed with theoretical random Mackenzie's distribution – (g-i).

3.3. Side surface analysis

Intermediate examination of the side surface showed that the large primary cracks emanating from the notch were formed in all investigated materials when the first-step loading accompanied by the in-situ hydrogen charging was interrupted somewhat beyond the ultimate tensile stress, Fig. 3a-c. In addition, the secondary cracks surrounding the primary ones were produced in all specimens, Fig. 3d-f. These cracks were found only within the plastic zone associated with the notch and the primary crack. The rest of the specimens' surface, which was

not deformed during tensile testing, was free of any hydrogen-related flaws. As can be seen in Fig. 3 the number of secondary cracks strongly depends on the material. The steel specimen is featured by numerous secondary cracks, Fig. 3c, f, while just a few secondary cracks are found on the side surface of the iron and Fe-Si alloy specimens, Fig. 3a and b. Apparently, the significantly higher propensity of steel to secondary cracking is related to the vast number of carbides, which are known to serve as the initiating points for HICs [43]. For all the materials, the primary and secondary cracks are mainly transgranular (TG). Nevertheless, the Fe-Si alloy has obviously a higher susceptibility to intergranular (IG) HAC than the two other materials, as is indicated by many IG and mixed-mode TG/IG secondary cracks, c.f. Fig. 3e. Many of TG cracks are largely curved and occasionally demonstrate the specific S-shape, e.g. Fig. 3f, which was recently found to be the characteristic feature of QC cracks in steel and iron [43,44].

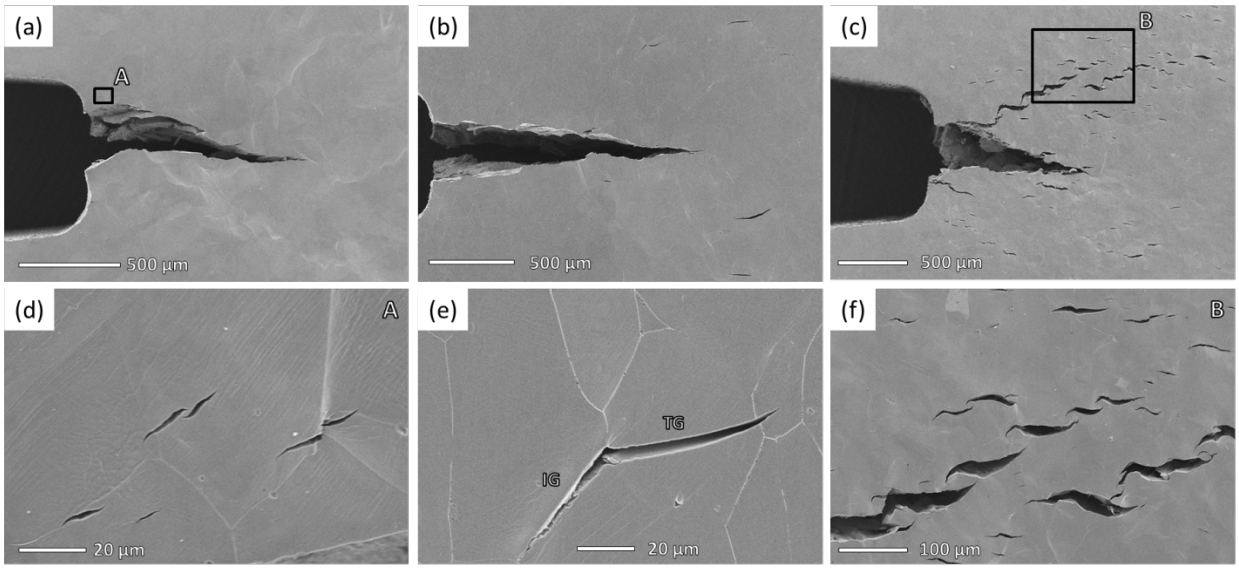

Fig. 3 – The SEM images obtained by the intermediate side surface examination revealing the primary – (a-c) and secondary – (d-f) cracks in pure iron – (a, d), Fe-2.5%Si alloy – (b, e) and low-carbon steel S235JR – (c, f) after the first-step tensile testing. The magnified images of the areas outlined by latter-labelled frames “A” and “B” in images (a) and (c) are represented in (d) and (f), respectively.

Since the second-step loading was conducted in liquid nitrogen, the fracture mode switched from QC to TC at this step. Thus, the post-mortem side surface examination, which was done after the second-step loading, permitted to outline the features intrinsic to each fracture mode across the same specimen. In particular, the comparison of the SEM images obtained by the intermediate and post-mortem side surface examinations made it possible to document the

evolution of the cracks path in the transition region between the fracture modes associated with the two steps of mechanical testing. SEM images obtained in this way for iron specimen are represented in Fig. 4. Figure 4a shows the tip of the primary QC crack, which was arrested at the interruption of the first-step loading. During the second-step loading, this crack propagated through the rest of the specimen by the TC mode. Thus, the specimen, as well as the side surface region shown in Fig. 4a, was broken into two halves. The upper and bottom parts of this side surface region are shown in Figs. 4b and c, respectively. Two non-metallic inclusions on all images in Fig. 4 are marked by the numbered arrows and serve as the reference points. It follows from the obtained images that the primary crack growth direction changed by 24° as soon as the second-step loading was started. This is illustrated by the red and blue dashed lines in Fig. 4c, which are associated with the traces of the QC and TC parts of the crack, respectively. Besides, the obvious misorientation of the corresponding QC and TC facets on the fracture surface can be seen in Fig. 4b and c. Since TC cracking in bcc iron occurs along the {100} planes, the cleavage crack growing within the same crystal may turn to 90 degrees angle only. Thus, when two segments of the same crack (one of which is unambiguously associated with TC) are spatially misoriented within a single crystal, and the angle between them is far from 90 degrees, one can conclude unequivocally that these segments have different crystallographic orientations. Apparently, this statement is correct only if both segments do belong to the same grain (crystal), the crystallographic orientation of which is not significantly distorted by plastic deformation. Unfortunately, the region of the side surface shown in Fig.4 was not suitable for successful EBSD analysis, so that the direct determination of the crystallographic features of the grain containing the crack was not possible. Nevertheless, in the specific case considered in Fig. 4, it can be shown with no aid from EBSD that the considered TC and QC parts of the crack were formed within the same grain. In particular, it is indicated by the slip line traces, marked by white dotted lines in Fig. 4a and c. As can be seen, these slip lines extend below both the QC and TC parts of the crack without any notable change of their orientation or geometry. One should also notice that these slip lines already existed in the grain before the second-step loading, so they are not resulted from any process during TC cracking. Thereby, it can be concluded that the QC and TC parts of the crack in Fig. 4b and c, most likely, have different crystallographic orientations. Furthermore, the QC crack exhibits very uneven and ragged edges, which can hardly be associated with any specific crystallographic plane, whereas the edges of the TC crack are perfectly straight as is reasonably anticipated.

Figures 5a and b demonstrate the side surface region of the steel specimen, which was observed during the intermediate and post-mortem SEM examinations, respectively. As follows

from Fig. 5a, this region contains one IG and one TG QC secondary cracks after the first step-loading. The new secondary TG crack and the fracture surface corresponding to the primary TC crack have appeared after the second step-loading, as one can see in the bottom of the image, Fig. 5b. In contrast to the QC crack having a characteristic curved shape, the new secondary crack exhibits an obviously sharper, thinner and straighter geometry, which is typical of TC cracks. According to the EBSD inverse pole figure (IPF) coloured map of the same region, Fig. 5c, both the QC and TC secondary cracks correspond to the same grain, demonstrating the uniform crystallographic orientation insignificantly distorted by plastic deformation. As has been already stated above, the TC cracking in bcc iron and steels occurs primarily along the {100} crystallographic planes. The cracks aligned with the crystallographic planes of this family must be either parallel or perpendicular to each other within an individual crystal. In harmony with this rule, the secondary and primary TC cracks shown in Fig. 5b are parallel to each other as well as to the traces of the {100} planes, which are indicated by the white dashed line in Fig. 5c. In contrast, the QC crack is misoriented with the TC cracks as well as with the {100} traces by about 18 degrees. The angle of misorientation between the QC and TC cracks far from 90 and 0° suggests their different crystallographic orientations, though it is generally questionable whether the strongly curved QC crack can be considered crystallographic at all.

Interestingly, the evidence for the different crystallographic orientations of the QC and TC cracks has also been obtained using the Fe-Si alloy, despite the frequently reported intrinsic propensity of this alloy to {100} cracking [13,14,16]. Figure 6 illustrates the evolution of the side surface region of the Fe-Si specimen during the two-steps mechanical testing. After the first-step loading, this region contained a few QC cracks, including the primary one, which are marked by the correspondingly labelled arrows in Fig. 6a. As can be seen in Fig. 6b, after the second-step loading, the extending of the primary QC crack by the TC mechanism resulted in the formation of the unified fracture surface. Besides, two new mutually parallel secondary TC cracks were introduced into the grain labelled by 1 in Fig. 6. This grain was also fractured by the primary QC crack during the first-step loading, c.f. Fig. 6a. As follows from the EBSD IPF map, acquired from this region and represented in Fig. 6c, the orientation of these TC cracks expectedly coincides with the traces of {100} crystallographic planes. As opposed to that, the orientation of the QC primary crack within the same grain mismatches with that of both the TC cracks and {100} planes by the approximately 30° degrees angle. Thus, the TC and QC cracks in grain 1 should have different crystallographic orientations. It is worth noting that, besides the cases considered above, the orientation of QC cracks occasionally coincides with that of TC cracks and planes. For example, in Fig. 6c, one can see that the edge of the primary QC crack is

nearly parallel to the traces of {100} planes in grains 2 and 3. Moreover, in grain 2, it is also parallel to the underlying TC crack. Thereby, the obtained results confirm the literature data in that the crystallographic orientation of QC HAC may or may not match that of TC.

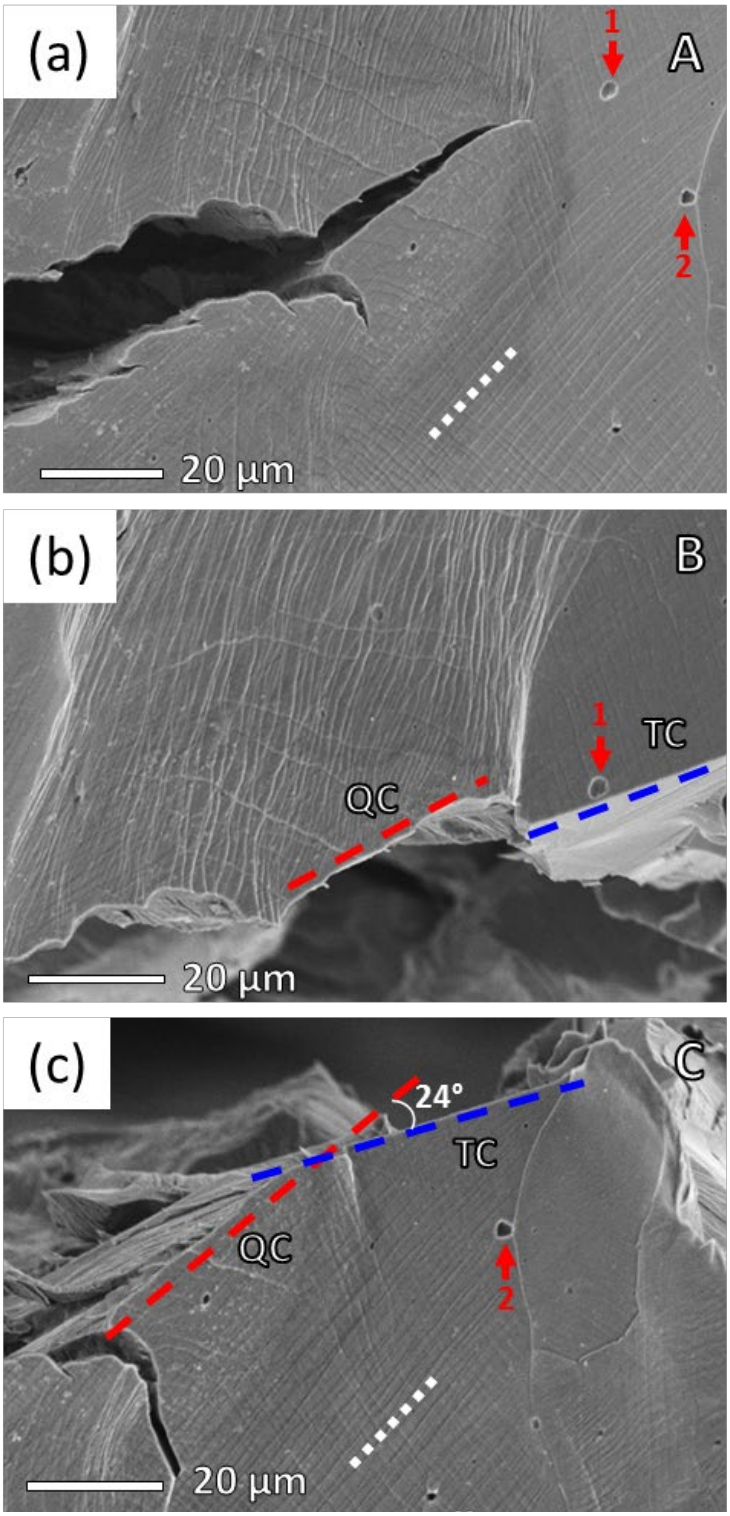

Fig. 4 – The SEM images demonstrating the specific region of the side surface of the pure iron specimen after the first- – (a) and second-step loadings – (b, c). The QC crack being arrested after the first-step loading (a) was extended by TC cracking during the second-step loading (b, c)

The red and blue dashed lines indicate the parts of the crack associated with QC and TC fracture modes respectively. The white dotted lines in (a) and (c) indicate the orientation of the specific slip lines. The non-metallic inclusions marked by numbered arrows can be used as the reference points.

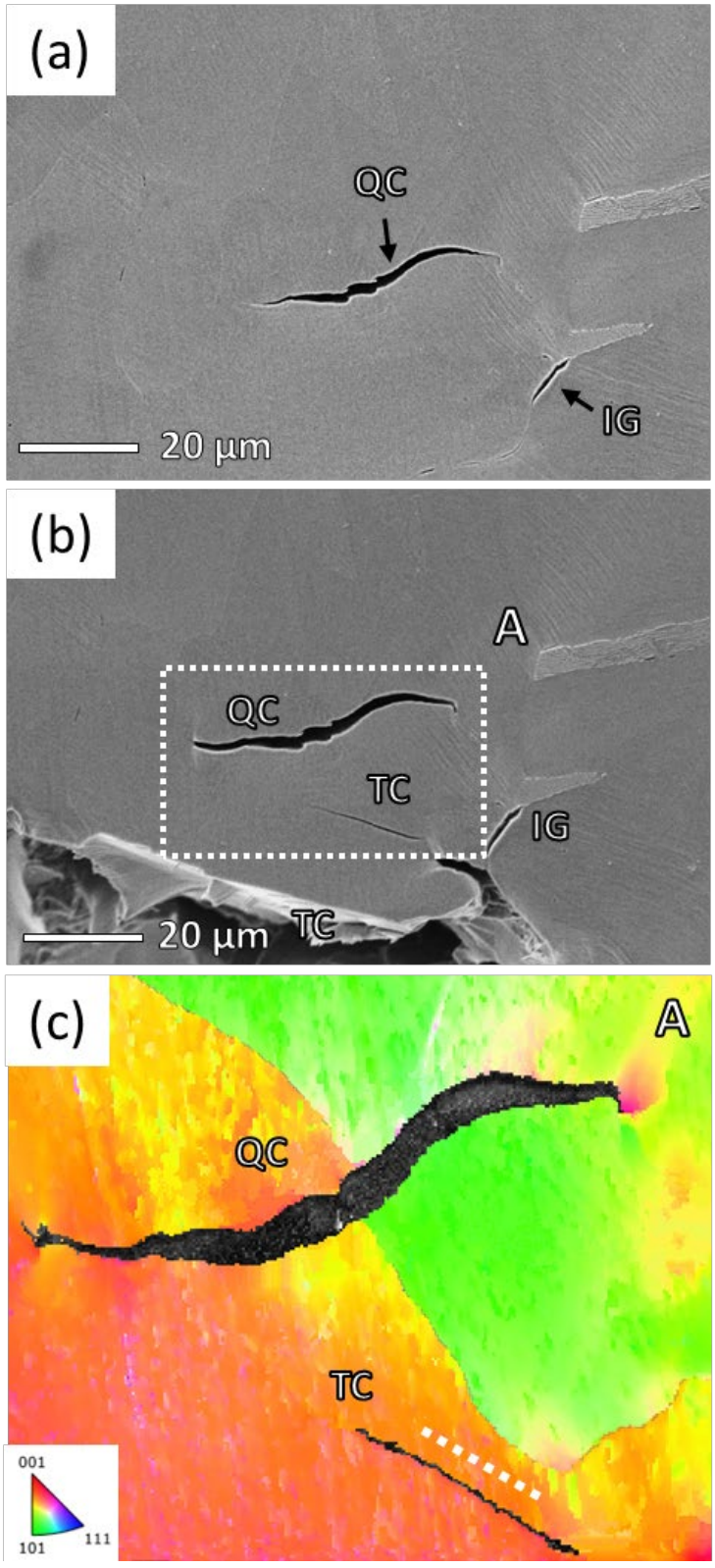

Fig. 5 – SEM images – (a, b) and EBSD IPF colour-coded map – (c) demonstrating the specific region of the side surface of the low-carbon steel S235JR specimen after the first- – (a) and second-step loadings – (b, c). The region represented in (c) is the magnified area outlined by "A" - labelled frame in (b). The white dotted line in (c) indicates the trace of the {100} crystallographic planes.

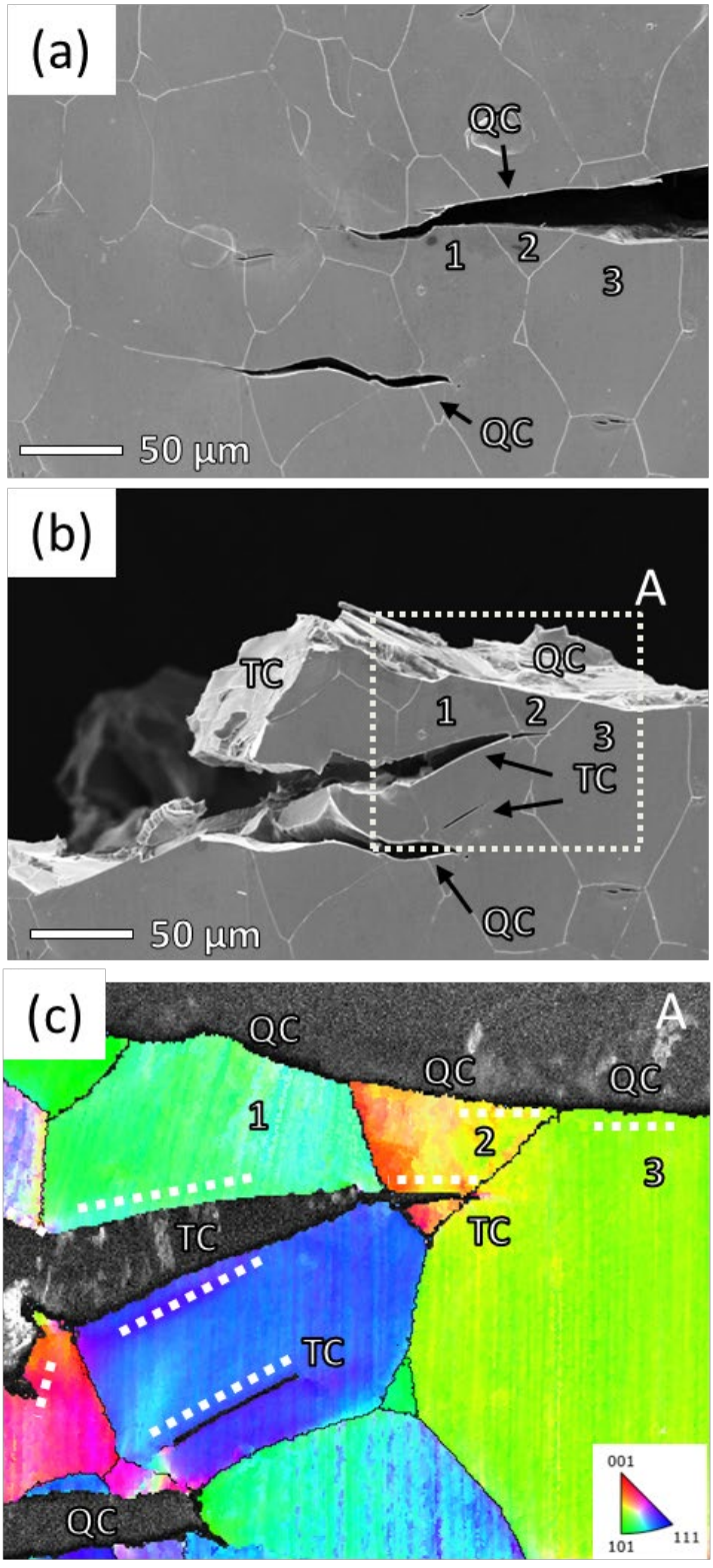

Fig. 6 – SEM images – (a, b) and EBSD IPF coloured-coded map – (c) demonstrating the specific region of the side surface of the Fe-2.5%Si alloy specimen after the first- – (a) and second-step loadings – (b, c). The region represented in (c) is the magnified area outlined by "A" - labelled frame in (b). The white dotted lines in (c) indicate the trace of {100} crystallographic planes.

Another important point to note is the considerably higher degree of plastic strain accompanying the QC HAC in all investigated materials in comparison to that associated with the TC cracking at the second-step loading. In Fig. 4b, one can see numerous intersecting slip lines surrounding the QC part of the crack. However, their density is abruptly reduced as soon as the TC mechanism is triggered during the second-step loading. For further illustration of this effect on the scale of the entire crack path, the panoramic height maps of the specimens side surfaces were obtained by CLSM. In the images represented in Fig. 7, the magnitude of plastic strain, as well as the size of the plastic zone under the primary crack path, can be assessed by the difference in the surface height. The undeformed part of the specimen has the maximal height, as is indicated by the red colour. Since the specimen experiences the reduction of the cross-section during tensile testing, the plastically deformed surface has a lower height with respect to the undeformed part of the specimen. According to the images shown in Fig. 7, the degree of plastic strain increases along the crack growth direction until the boundary between the QC and TC parts of the crack, where the maximal strain is observed for materials examined. The side surface of the specimens under the TC part of the crack exhibits lower strains. Thus, it is obvious that the propagation of the TC crack was accompanied by considerably less plastic deformation if compared with the QC crack, which is again a plausible result.

3.4. Fractographic analysis

The entire fracture surfaces of the iron, Fe-Si alloy and steel specimens, which have undergone the full cycle of the two-step tensile testing, are represented on the SEM images in Figs. 8a, b and c, respectively. It follows from Fig. 8 that all fracture surfaces exhibit two distinct regions with a clear boundary between them. In all specimens, the length of the first region, starting from the notch, is found to have coincided with the length of the primary crack measured during the intermediate SEM examination. Thus, this region was obviously produced by HAC during the first-step loading accompanied by hydrogen charging. Consequently, the other region corresponds to the second-step loading conducted in liquid nitrogen. It is found that, on the scale of the entire fracture surface, the second region demonstrates a much more uneven relief in comparison to the first one produced by HAC. To illustrate this observation, the characteristic

CLSM topographic profiles are provided under the corresponding fractographic images in Fig. 8. The profiles were taken along the dash-dotted lines shown on the fracture surface images. It is apparently seen that the profile of the first region is much plainer than that of the second region.

The fractographic analysis of the specimens performed at higher magnification showed that the first region is composed of the transgranular facets exhibiting the attributes characteristic of the QC morphology - the quite rough micorelief, the tear ridges alternating with the flat terraces and the striations oriented across the crack growth direction, c.f. Figs. 9a, c, e. The second region is represented solely by the TC facets featured by classical river patterns as well as by the less rough relief and more clear boundaries in comparison to those of the QC facets, c.f. Figs. 9b, d, f. The morphology of the facets of both kinds is not found to be appreciably influenced by the material, while their size correlates strongly with the diameter of the grains of a given material, as can be seen in Fig. 9 and Table 2. The largest average size of facets is observed in iron having the largest grain size, while the smallest facets are found in the steel specimen with the smallest grain size. Nevertheless, the size of facets is always smaller than that of grains by approximately 1.8 times. This indicates that more than one facet is normally produced within one grain. The size of the QC facets is commonly slightly larger than that of the TC ones.

Table 2 – The quantitative parameters characterising the microstructure and fracture surfaces of different kinds in the investigated materials.

Material	Technically pure iron		Fe-2.5%Si		Low-carbon steel*	
Average grain diameter (d_g), μm	79		52		36	
Fracture mode	TC	QC	TC	QC	TC	QC
Average facet diameter (d_f), μm	43.5 (±6.6)	55.0 (±7.6)	26.9 (±4.0)	29.1 (±2.7)	19.5 (±2.2)	24.5 (±0.7)
Average angle of misorientation between adjacent facets (θ_f), º	38.1 (±6.6)	20.7 (±2.2)	29.5 (±3.2)	18.9 (±2.1)	35.7 (±2.3)	23.3 (±1.1)
Roughness of a fracture surface (S_q), μm	10.1 (±1.8)	4.1 (±1)	13.7 (±2.0)	6.8 (±1.5)	14.4 (±3.8)	6.9 (±1.6)
Mean standard deviation of the facet's surface relief from the	1.33 (±0.28)	1.74 (±0.26)	0.55 (±0.31)	0.92 (±0.15)	0.46 (±0.06)	1.27 (±0.18)

approximating plane (D), μm	

*adopted from [38]

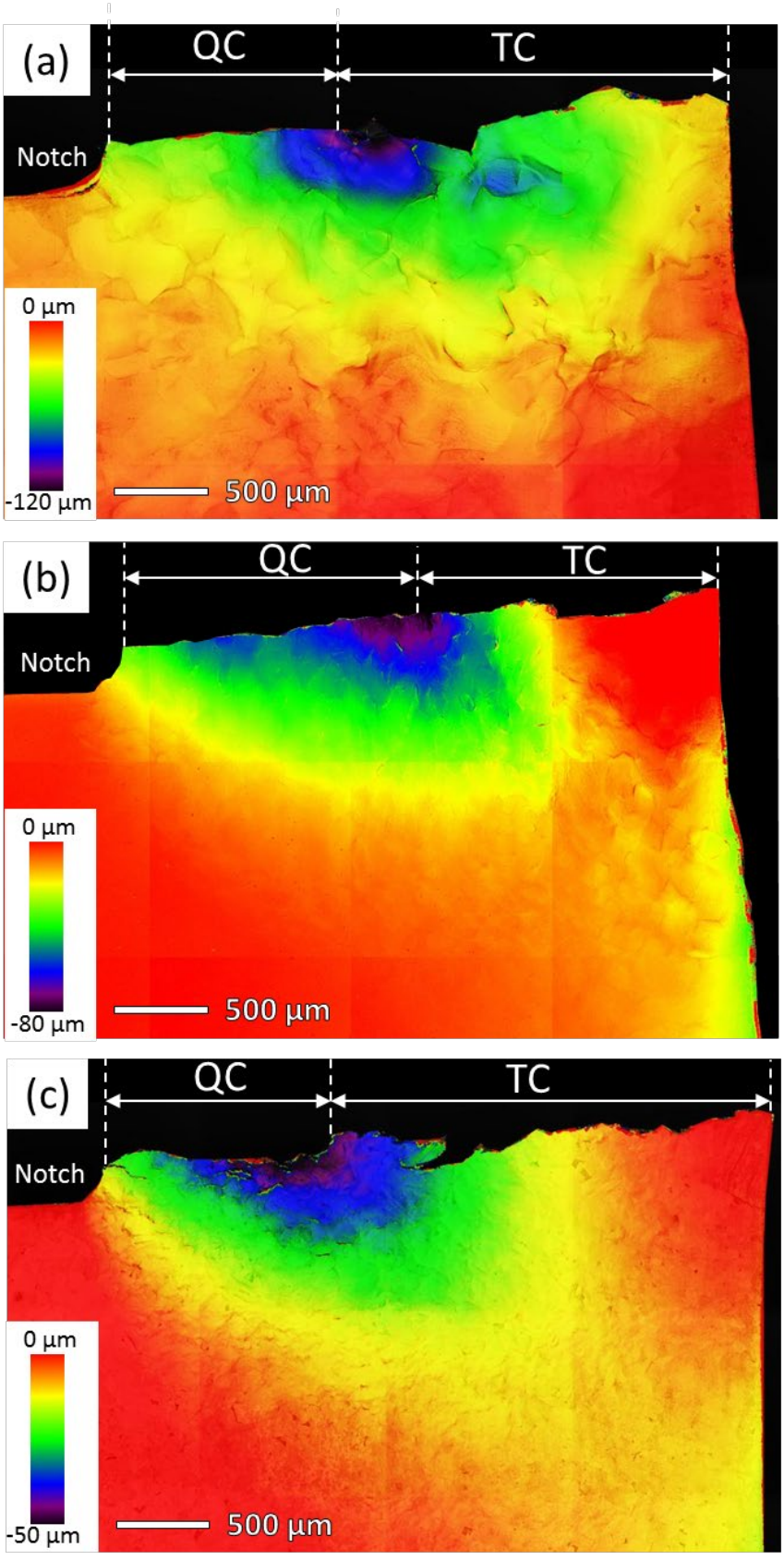

Fig. 7 – The height maps obtained by CLSM from the side surfaces of the technically pure iron – (a), Fe-2.5%Si alloy – (b) and low-carbon steel S235JR – (c) specimens.

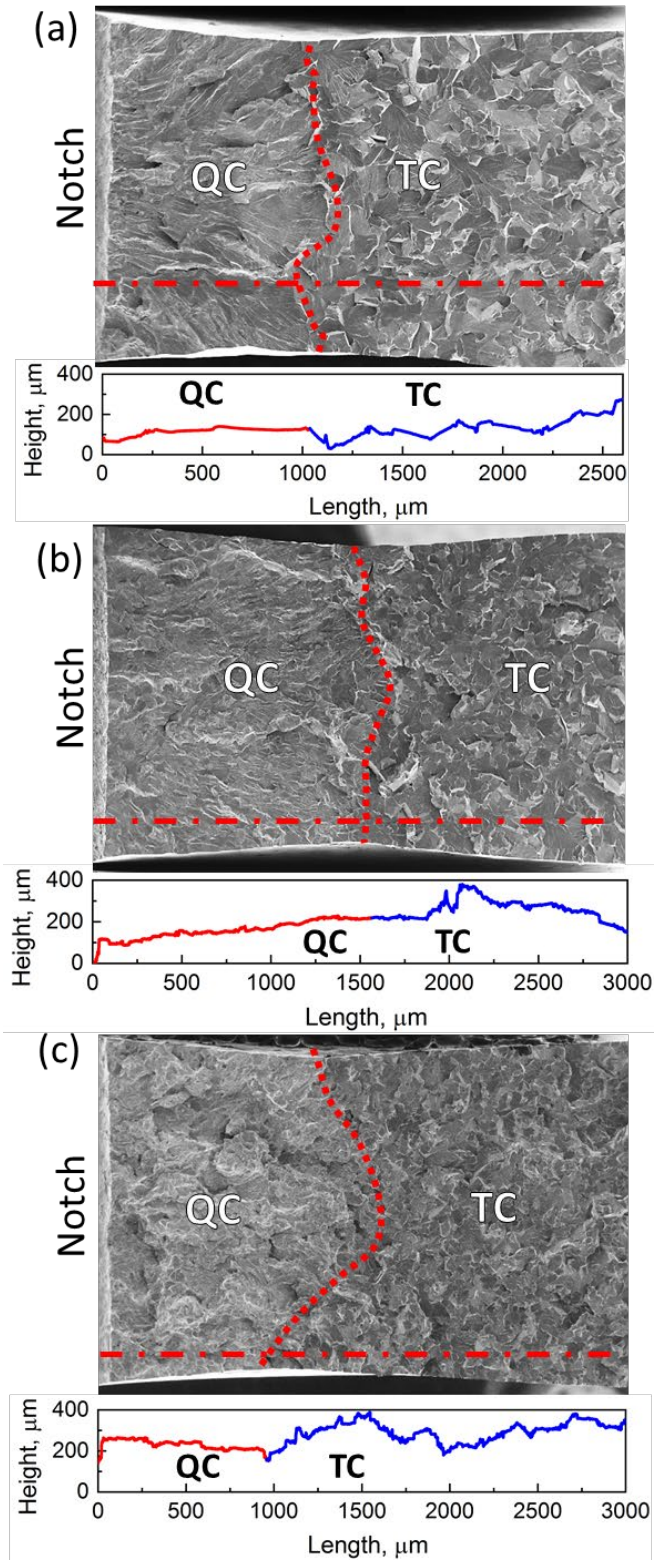

Fig. 8 – The entire views of the fracture surfaces of the technically pure iron – (a), Fe-2.5% Si alloy – (b) and low-carbon steel S235JR – (c) specimens underwent the full cycle of the two-step tensile testing. The diagrams below the SEM images represent the topographic profiles

obtained by CLSM along the dash-dotted lines provided on the corresponding fractographic images. The dotted curves indicate the boundary between the QC and TC regions

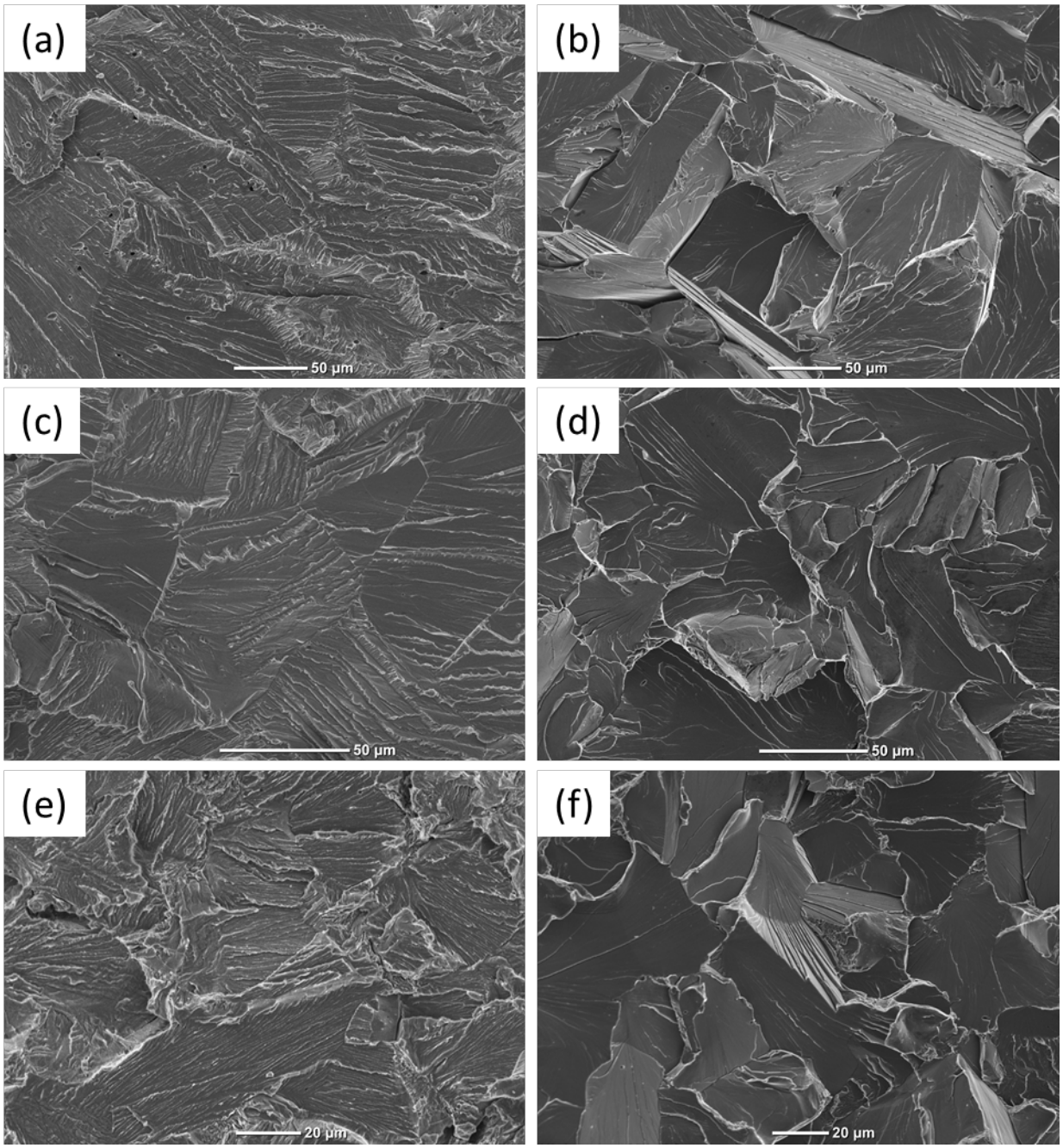

Fig. 9 – The morphology of QC – (a, c, e) and TC – (b, d, f) regions on the fracture surfaces of the technically pure iron – (a, b), Fe-2.5%Si alloy – (c, d) and low-carbon steel S235JR – (e, f) specimens.

It should be stressed that no notable transition region on the fracture surface between the two fracture modes is found in all materials tested, c.f. Fig. 10. The boundary demarcating the QC and TC morphologies is always unequivocally defined and, according to the side surface examination, is often observed within the grain interior, c.f. Fig.4-6. Since the dislocation density

within a crystal cannot be changed quickly in a step-wise manner, the transformation of the QC morphology into the TC one cannot be simply explained by the different extent of plastic strain in the microstructure. This observation indicates that plastic deformation, which had been developed ahead of the QC crack during the first-step loading, does not significantly affect the morphology of TC facets. Thus, the features of QC and TC morphologies are attributed to the different mechanisms of crack growth and not to the preliminary plastic strain in the microstructure.

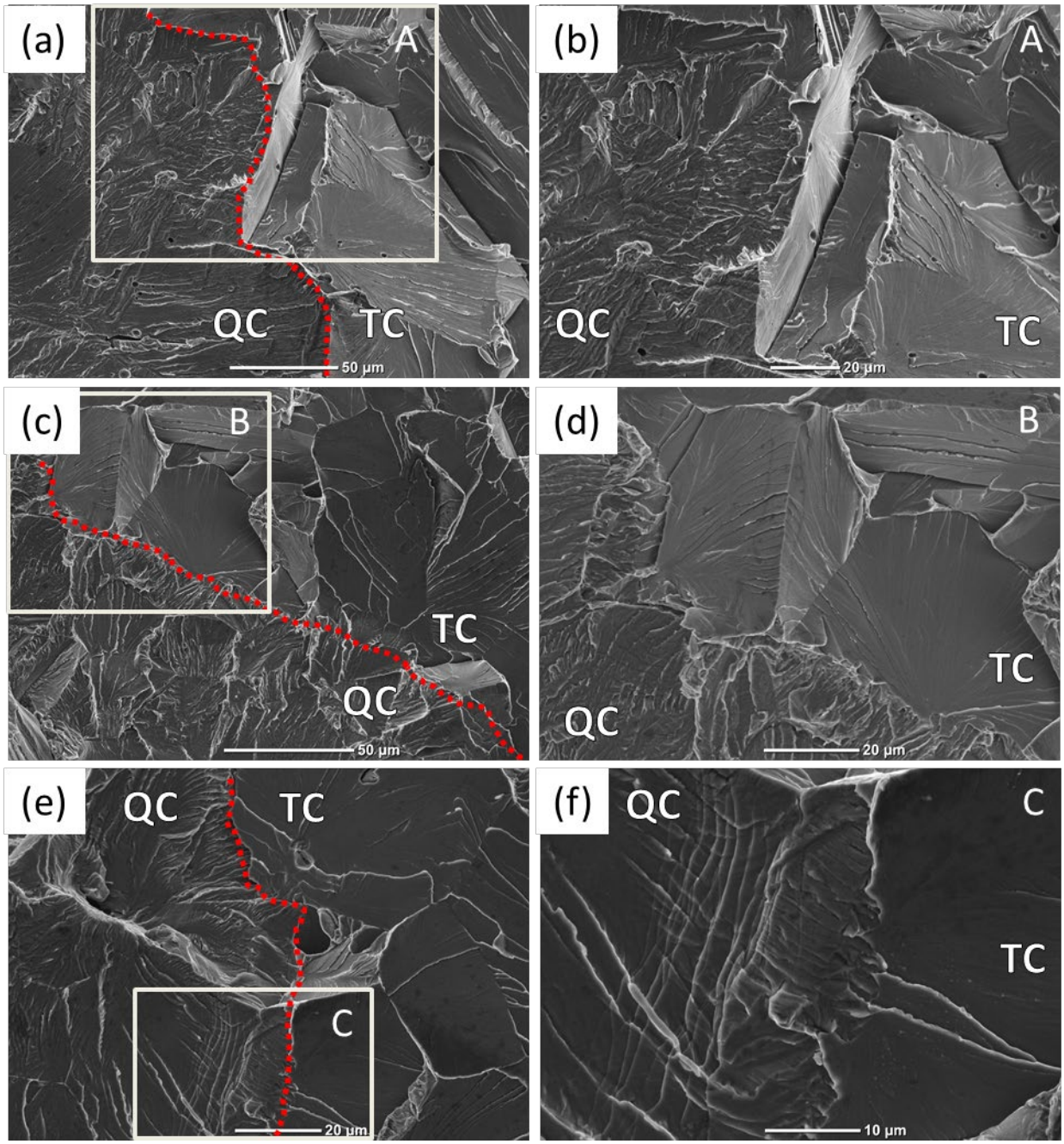

Fig. 10 – The morphology of the fracture surface at the boundary between the QC and TC regions in the technically pure iron – (a, b), Fe-2.5%Si alloy – (c, d) and low-carbon steel

S235JR – (e, f) specimens. The magnified areas outlined by letter-labelled frames “A”, “B” and “C” on images (a), (c) and (e) are represented on figures (b), (d) and (f), respectively. The dotted curves on images (a), (c) and (e) indicate the boundary between the QC and TC regions

To illustrate the topographic features of the QC and TC fracture surfaces on the scale of a few facets, the 3D CLSM images and corresponding topographic profiles are shown in Fig. 11. It can be seen from Fig. 11 that in harmony with the results obtained in our previous studies, the QC surfaces in all the investigated materials possess the characteristic “hills-like” topography attributed to the smoothly curved QC facets. As opposed to that, the TC parts of the fracture surfaces are featured by the “alpine-like” profiles. The “slopes” in the profiles correspond to TC facets misoriented at widely ranging angles, while the “peaks and valleys” represent the joints of these facets. It should be noted that not all the QC facets are curved. Many of them have a relatively flat surface resembling that of TC facets. However, as follows from Table 2, the QC facets have more pronounced unevenness on average than the TC ones, as is quantitatively indicated by the higher average values of the D parameter representing the deviation of the individual facets relief from the approximating plane. Thus, in comparison with that of TC, on the scale of one facet, the relief of QC has a notably larger roughness. Nevertheless, on the scale of several facets, the roughness of the QC surface is lower than that of TC as summarised in Table 2.

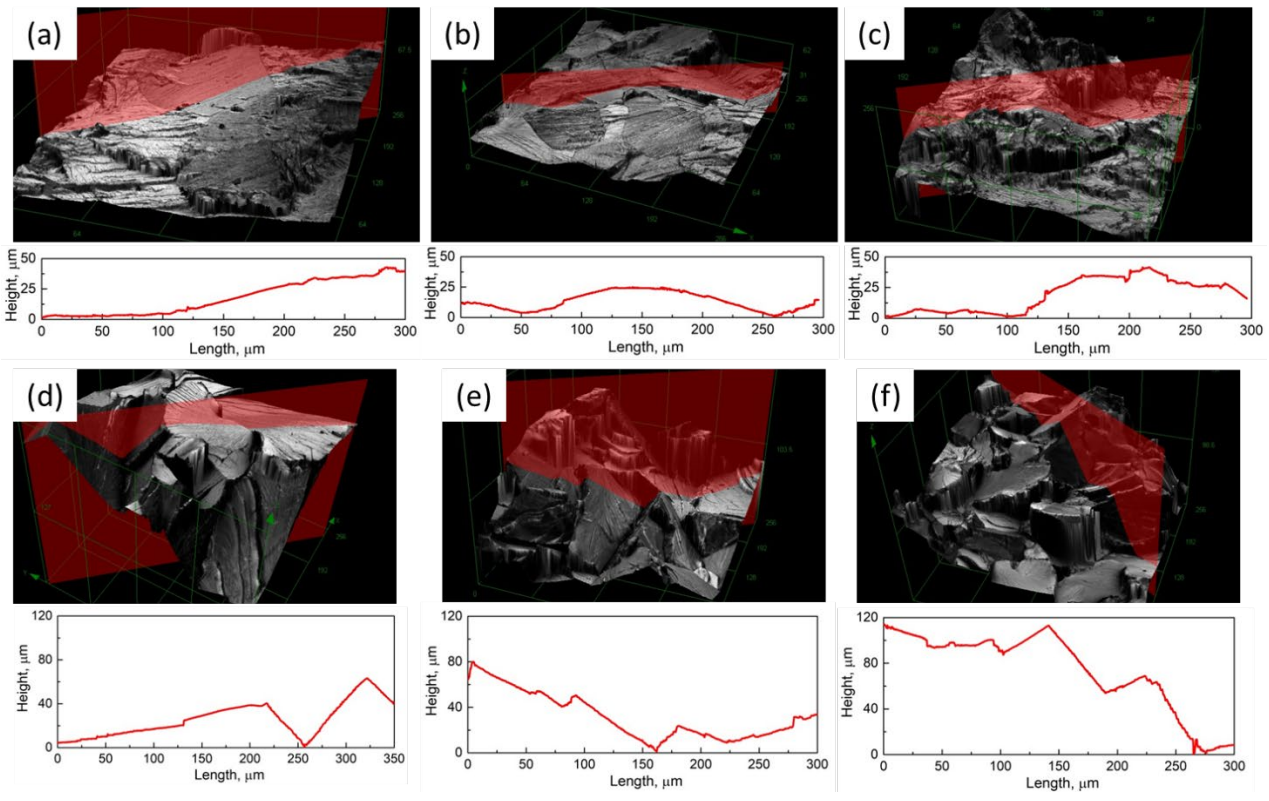

Fig. 11 – The 3D CLSM images with corresponding topographic profiles for QC – (a-c) and TC – (d-f) regions on the fracture surfaces of the technically pure iron – (a, d), Fe-2.5%Si alloy – (b, e) and low-carbon steel S235JR – (c, f).

It is established that the roughness of the QC and TC surfaces is largely attributed to the misorientation of the facets. The quantitative analysis showed that depending on the material, the average AMs of the QC and TC facets are in the ranges of 18.9-23.3° and 29.5-38.1° respectively, see Table 2. Thus, on average, the AM of the QC facets are 1.5-2 times lower than that of the TC ones. Besides, it is found that the distributions of the angles of misorientation (DAM) corresponding to the two kinds of facets have completely different features, c.f. Fig. 12. It is found that for all materials studied, the DAMs of QC facets exhibit characteristic lognormal shape with one distinct peak at around 15°, Fig. 12a-c. The AMs of QC facets generally do not exceed 70-75°. In contrast, the AMs between the TC facets are ranged from 0 to 90°, c.f. Fig. 12d-f, while the dominating peak in the DAMs appears at 29-39.5°, depending on the material. Two other modes can be distinguished in the low- and high-angle domains of the DAMs of TC facets. The high-angle mode is observed approximately in the 70-90 degrees range and is much lower by magnitude in comparison with two other modes. Presumably, this mode can be attributed to the facets belonging to the same grain. The cleavage crack, which must turn along the equal {100} crystallographic plane within the same grain, should result in the formation of two TC facets orientated at 90° angle to each other. The TC facets of this kind have been frequently observed in the present and previous studies, c.f. Fig. 10d. In particular, the most pronounced high-angle mode on the DAM was observed in the iron specimen, which has the largest average grain size among the investigated materials. Indeed, in the large grain, the probability of the formation of several TC facets is reasonably anticipated to be higher. The magnitude of the low-angle mode is comparable with that of the dominating one. The notable prevalence of the TC facets with AMs of 0-45° in all investigated materials is evident from the DAMs shown. The exact nature of the low-angle mode is still unknown. However, we suppose that it can be related to the cleavage fracture along the sub-grains with low-angle boundaries, which are likely produced by plastic deformation. It is obvious from Fig. 7 that the TC crack propagated through the specimen, which had been already considerably deformed plastically during the first-step loading. The fragmentation of ferritic grains by the process of plastic deformation is well expected. In our previous study [41], the low-carbon steel (the same as that used in the present work) was fractured in liquid nitrogen with no preliminary straining. In that case, the DAMs of TC facets featured by the significantly lesser fraction of low AMs than in the

present investigation. This fact likely corroborates the suggestion on the relation between plastic deformation and the low-angle mode of the DAMs of TC facets.

It should be noted that the smallest average angles of misorientation for both the QC and TC facets correspond to the Fe-Si alloy. The probable reason for that is the slightly lower overall misorientation of the grains in this alloy, c.f. Fig. 2h. However, this suggestion requires additional verification, which was beyond the scope of the present study.

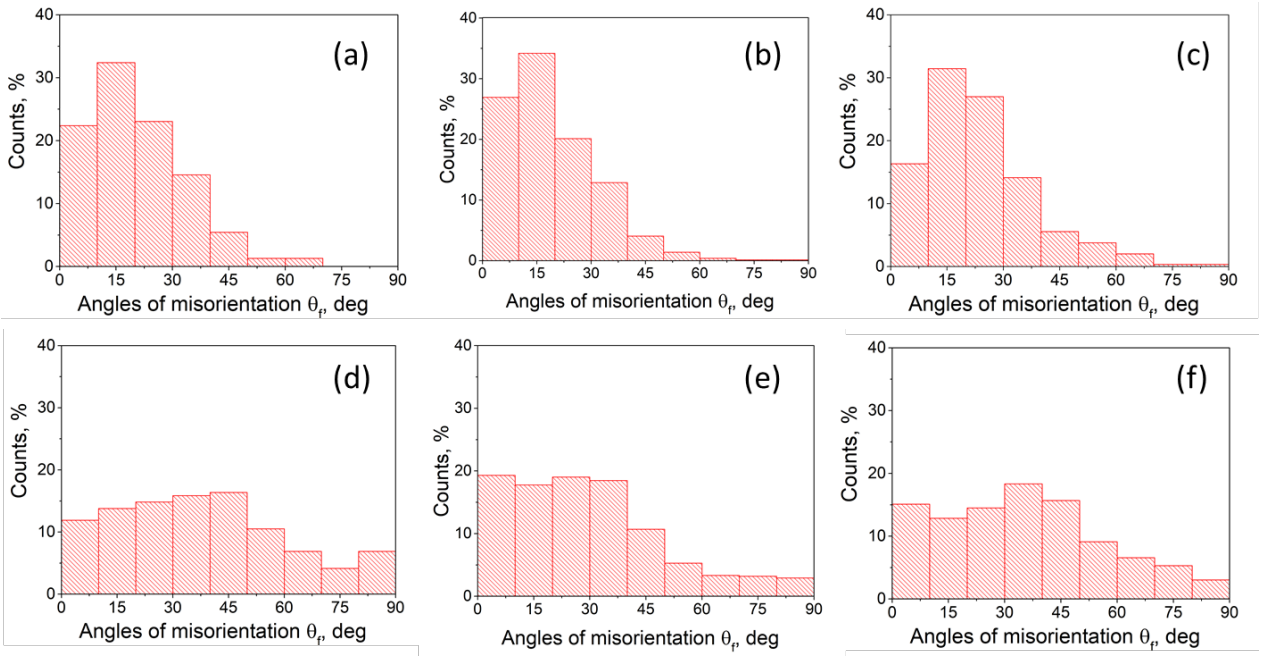

Fig. 12 – The distributions of the angles of misorientation between adjacent QC – (a-c) and TC – (d-f) facets on the fracture surfaces of the technically pure iron – (a,d), Fe-2.5%Si alloy – (b, e) and low-carbon steel S235JR – (c, f) specimens.

4. Discussion

The results obtained in the present study show that the average angle of misorientation between the adjacent QC facets produced by HAC in iron, Fe-Si alloy and steel is significantly lower than that of the TC facets belonging to the same fracture surface. Besides, the angles of misorientation exhibit fundamentally different distributions for QC and TC facets. These findings indicate that, in general, the orientation of QC facets with respect to the microstructure and to the crystallographic orientation of grains is significantly different from that of the TC ones in all investigated materials. This conclusion is well supported by the side surface examination, which confirms that many QC and TC secondary cracks being observed even within the same grain possess notably different crystallographic orientations. Consequently, the QC HAC should

occur mainly out of the {100} crystallographic planes, i.e. primary TC planes in bcc iron and its alloys. Although it may seem so, the conclusion made does not contradict the results of the other studies, which reports the {100} orientation of QC fracture surfaces produced by HIC [13,14,27], HAC [6,15,16,29,32,33] and HAFCG [18,30,34]. According to the abundant literature, the QC HAC indeed occurs always along the {100} crystallographic planes in bcc iron and Fe-Si single crystals at room temperature [6,16,29,32,33]. However, it is the case only if the notch and {100} planes of the single crystal specimen are perpendicular to the tensile axis. It was established that in the absence of the notch or in the case when the {100} planes of the single crystals are not normal to the tensile axis, the path of QC HAC or HAFCG can significantly deviate (at least on the macroscale) from the {100} planes as well as from any other crystallographic planes [7,29,31–33]. In fact, the literature data suggest that regardless of the orientation of the single crystals, the QC crack tends to align itself with the plane of normal stress, even though the large deviation of the crack path from specific crystallographic planes can occur in such conditions. The materials used in the present study have a random misorientation between grains. As the primary macro-crack propagates through the random grain microstructure, it consistently meets the grains, which are arbitrarily oriented to its tip as well as to the tensile axis. Thus, it is reasonable to suggest that the tortuosity of the QC crack path, which is not confined to the {100} planes only, should be much less in comparison to that of the TC crack, which must grow primarily along the {100} planes. In other words, compared to the TC cracks, the QC crack possesses much higher flexibility to align itself with the macro-plane of fracture. This characteristic feature of the HAC is well supported in the present study by low angles of misorientation between the adjacent QC facets as well as by low roughness of the QC part of the fracture surface on the scale equal to or larger than a few facets. It should be noted that although the results of the present study testify the QC HAC out of the TC planes, the involvement of {100} crystallographic planes in this process is not excluded from the HAC process. The significant evidence accumulated in the literature leaves no doubts that QC HAC can occur along the {100} planes in all ferritic materials. We showed that QC and TC crack could occasionally grow along with the same family of planes. However, we suppose that in the polycrystalline material, this happens only in the situation when the grain is favourably oriented with respect to the crack path and the tensile axis. Taking into account the considerably lower average value of AMs and the dramatically different distribution of AMs of the QC facets in comparison to TC ones, one may presume that such a situation is rare. Thus, by the most, the QC HAC occurs out of the TC planes. This observation implies a fundamental difference in the mechanisms underlying the two fracture modes investigated. It also tacitly challenges the role of cleavage-

like mechanism in the QC HAC. In view of aforesaid, the morphology of QC on the finer scale is of interest.

The results of the present study evidently show that on a scale equal to or larger than several neighbouring facets, the spatial out-of-plane deviation of the QC HAC path is much lower than that of TC unstable cracking. However, the inverse behaviour is observed on the scale of an individual facet. In all the materials investigated, the QC facets, on average, demonstrate a larger dispersion of approximation by a plane in comparison with the TC ones. This indicates the greater deviation of the microrelief of the QC facets from the perfect crystallographic planes. The uncertain crystallographic orientation and the significant unevenness of QC surfaces were observed in many studies [7,17,29,32,33,37], including our recent reports [41,43]. The curved QC secondary cracks were also demonstrated in the present paper. Nevertheless, the larger unevenness of the QC facets can be explained in two different ways. For example, Vehoff and Rothe [29] stated that even though the QC fracture surface of the Fe-2.6% Si single-crystal appeared to be macroscopically aligned with the {110} plane, in fact, it was produced by HAC along the microscopic {100} terraces oriented at high angles to the macroscopic plane of the fracture surface. Similar sub-facets providing substantial roughness to the QC fracture surface were also observed by other researchers. That is the QC HAC, which occurs by the unstable TC increments producing largely misoriented small terraces with the {100} orientation, can be the one reason for the increased roughness of the QC facets. Nevertheless, in the present investigation, as well as in our previous studies [41,43] it was shown that some of the QC cracks and facets have essentially smoothly curved surface profiles, thus exhibiting virtually no steps or terraces. Thereby, the mechanism other than TC should operate to produce the QC cracks. It was suggested in [43] that one of the plasticity-related mechanisms, e.g. AIDE, HELP or HESIV, can be responsible for this. Further investigations are required to elucidate the importance of these mechanisms in HAC. In particular, the high-resolution technique capable of in-situ observation of the crack wake during HAC is needed to establish the exact processes responsible for the formation of QC morphology.

Another important finding of the present study is that the orientation of QC facets is not significantly influenced by the chemical composition of the iron-based alloys. This observation conflicts with the previously reported findings that different crystallographic orientations of QC cracks in hydrogen embrittled iron, Fe-Si alloys, and low-carbon steels. We suppose that this contradiction can be simply explained by the small experimental datasets, which do not permit performing the reliable statistical analysis, and which are common in most early studies based on the conventional techniques used for the determination of crystallographic orientations of cracks

and fracture surfaces. The method used in the present study is free of such limitations. The analysis is based on statistically representative datasets. Therefore, the inferred conclusions are considered to be technically sound. However, the difference in the methodological approach can be not the sole reason for the discrepancy between the results of the present work and those reported by other researchers. Probably, the crystallography of the QC surface depends not only on the chemical composition but also on the experimental conditions at which this surface was formed. For example, Nakasato and Bernstein [14] showed that the crystallography and mechanism of HIC in the single and bi-crystals of Fe-Si alloys strongly depend on the concentration of Si. They found that in pure iron, the HICs had the QC morphology and were aligned with the {110} and {112} planes, while in the Fe-3%Si alloy, the HICs exhibited the TC appearance and the {100} orientation. Several other researchers also found that HIC in single crystals of Fe-3%Si alloy occurs along the TC planes of the {100} family [13,27]. The results of the present investigation indicate that HAC in the polycrystalline Fe-Si alloy produces QC facets, the crystallographic orientation of which is notably different from that of TC and is practically the same as that of QC facets in iron and steel. It was established in [14] that the change from TC to QC HIC occurs at Si content of about 0.7%. Hence, the fact that in the present study, the concentration of Si was 2.5% and not 3%, as in other studies cited above, can hardly be considered significant enough for alternation of the fracture mode. Most probably, the difference in the crystallography of HAC and HIC is attributed to the specifics of the mechanisms governing these two phenomena. As was shown above, in the case of HAC, the crystallographic orientation of the QC facet within a given grain is largely predetermined by the spatial orientation of the primary macrocrack introducing to this grain from the preceded neighbouring one. In contrast to HAC, neither the external stress nor the presence of macro crack is a prerequisite for HIC. It is known that the latter phenomenon is driven by the high internal pressure of molecular hydrogen, which is recombined from atomic hydrogen accumulating within the discontinuities in the microstructure. At least at the early stage of hydrogen charging, HICs nucleate and propagate within the grains independently of each other and are not influenced by the far-field stress from the notch or macrocrack. Hence, the propagation direction of HICs is primarily determined by the configuration of the discontinuity filled with molecular hydrogen as well as by the intrinsic propensity of the specific alloy to a certain type of fracture. Even in the absence of hydrogen, Fe-Si alloys are known to be highly susceptible to the TC fracture, which is likely due to the weak interatomic bonds along the {100} planes. Hence, it can be supposed that in the absence of the notch or macrocracks, there are no factors tending to deflect the path of the HIC away from the intrinsically most favourable crystallographic planes, which correspond to the {100} family in the Fe-3%Si alloy and to the {110} and {112} families

in pure iron in accordance with [14]. However, in the case of HAC, the intrinsic propensity to the TC plane cracking probably can be interfered with or even completely suppressed by the influence of the far-field stress associated with the notch or macrocrack. Thereby, in contrast to that of HIC, the crystallography of QC HAC is rather weakly influenced by the chemical composition of the bcc iron-based materials.

The final remark should be made in regard to the possible effect of hydrogen on TC fracture. Due to the specifics of the experimental metod used in the present study, it cannot be excluded that a certain amount of diffusible hydrogen could retain in the specimens during testing in liquid nitrogen. Although, after the first-step loading, diffusible hydrogen rapidly evolves from the specimen, especially during the inetrmidiate side-surface examination when the specimen is placed in the vacuum chamber of the SEM, some strain-iduced traps such as dislocations and vacancies can probably bound an appreciable amount of hydrogen atoms. Whether this hydrogen affects the TC fracture or not is questionable. On the one hand, the diffusion rate of hydrogen at -196 ºC is insufficient to cause hydrogen embrittlement in a "common" way, which requires a redistribution of diffusible hydrogen in the microstructure followed by buildup of a very high concentration of hydrogen in local volumes. On the other hand, the reduction of the cleavage stress in pure iron single crystals by hydrogen has been reported even at such low temperatures [7]. Despite these concerns, there are strong arguments in favour that hydrogen unlikely profoundly affects the fracture mechanism and, consequently, the fracture surface morphology of the investigated materials tested in liquid nitrogen. The TC morphology of the specimens examined here is visually very similar to that of the hydrogen-free specimens tested in liquid nitrogen in our previous study [41]. Quantitatively, the average value and the distribution of angles of misorientation between TC facets in the present study is only slightly different (just by about 4 degrees) to those of TC facets from the ref. [41], where the hydrogen-free specimens were analyzed. Most likely this difference falls in the range of regular experimental scatter. However, one may also suppose that it can be attributed to the influence of retaining hydrogen or to the influence of the notch, since in the previous study the smooth specimens were used. Anyway, the observed difference is incomparable with the difference between the misorientation between QC and TC facets. Thus, in our opnion, it is unlikely that hydrogen (if presents in the metal at all) can significantly affect the features of the fracture surface at the liquid nitrogen temperature.

5. Conclusions

1. The fundamental difference between the QC HAC and the TC cracking in ferritic materials is in that, on the distance equal to or larger than several facets size, the former possesses the significantly lower out-of-plane deviation of the crack's path, whereas on the scale finer than the facet size this deviation is higher.

2. On the scale of the entire ferritic grain, the crystallographic orientation of the cracks produced by QC HAC may or may not match the TC crystallographic planes as evidenced by the SEM and EBSD side surface examination. Nonetheless, the QC HAC in polycrystalline ferritic materials mainly runs out of the TC crystallographic planes, as is statistically witnessed with high confidence by the substantially different distribution of angles of misorientation between adjacent QC facets as well as by their 1.5 - 2 times lower average value in comparison to those of TC facets.

3. The morphology, path and mechanism of QC HAC are essentially the same in polycrystalline pure iron, Fe-2.5%Si alloy and low-carbon steel.

4. Preliminary plastic deformation of ferritic grains cannot be responsible for the transition of the fracture surface morphology from the true cleavage to quasi-cleavage.

5. The mechanism of quasi-cleavage hydrogen assisted cracking in bcc iron or ferritic alloys is fundamentally different from the true cleavage, though the contribution from the latter cannot be fully excluded.

Acknowledgements

Financial support from the Russian Science Foundation through the grant-in-aid No. 19-79-00188 is gratefully appreciated. In addition, the authors wish to thank Andrey Kudryavtsev from TESCAN Ltd. for his kind help with the EBSD analysis.

Data availability

The raw/processed data required to reproduce these findings cannot be shared at this time as the data also forms part of an ongoing study.

List of references

[1] H.C. Burghard, N.S. Stoloff, Cleavage Phenomena and Topographic Features, in: C.D.

Beachem (Ed.), Electron Fractography, 1968: pp. 32–58.

[2] P. Mohseni, J.K. Solberg, M. Karlsen, O.M. Akselsen, E. Ostby, Application of combined EBSD and 3D-SEM technique on crystallographic facet analysis of steel at low temperature, J. Microsc. 251 (2013) 45–56. doi:10.1111/jmi.12041.

[3] J. Nohava, P. Haušild, M. Karlík, P. Bompard, Electron backscattering diffraction analysis of secondary cleavage cracks in a reactor pressure vessel steel, Mater. Charact. 49 (2002) 211–217. doi:10.1016/S1044-5803(02)00360-1.

[4] P.A. Davies, M. Novovic, V. Randle, P. Bowen, Application of electron backscatter diffraction (EBSD) to fracture studies of ferritic steels, J. Microsc. 205 (2002) 278–284. doi:10.1046/j.1365-2818.2002.00998.x.

[5] P.A. Davies, V. Randle, Combined application of electron backscatter diffraction and stereo-photogrammetry in fractography studies, J. Microsc. 204 (2001) 29–38. doi:10.1046/j.1365-2818.2001.00922.x.

[6] F. Terasaki, T. Kawakami, A. Yoshikawa, N. Takano, Mechanism of crack propagation due to hydrogen embrittlement in iron single crystals stressed along [001] axis, Rev. Metall. Cah. D'Informations Tech. 95 (1998) 1519–1529. doi:10.1051/metal/199895121519.

[7] A. Kimura, H. Kimura, Hydrogen embrittlement in high purity iron single crystals, Mater. Sci. Eng. 77 (1986) 75–83. doi:10.1016/0025-5416(86)90355-1.

[8] M.L. Martin, I.M. Robertson, P. Sofronis, Interpreting hydrogen-induced fracture surfaces in terms of deformation processes: A new approach, Scr. Mater. 59 (2011) 3680–3687. doi:10.1016/j.actamat.2011.03.002.

[9] M.L. Martin, J.A. Fenske, G.S. Liu, P. Sofronis, I.M. Robertson, On the formation and nature of quasi-cleavage fracture surfaces in hydrogen embrittled steels, Acta Mater. 59 (2011) 1601–1606. doi:10.1016/j.actamat.2010.11.024.

[10] E.D. Merson, P.N. Myagkikh, G.V. Klevtsov, D.L. Merson, A. Vinogradov, Effect of fracture mode on acoustic emission behavior in the hydrogen embrittled low-alloy steel, Eng. Fract. Mech. 210 (2019) 342–357. doi:10.1016/j.engfracmech.2018.05.026.

[11] E. Merson, A. Vinogradov, D.L. Merson, Application of acoustic emission method for investigation of hydrogen embrittlement mechanism in the low-carbon steel, J. Alloys

Compd. 645 (2015) S460–S463. doi:10.1016/j.jallcom.2014.12.083.

[12] M.C. Tiegel, M.L. Martin, A.K. Lehmberg, M. Deutges, C. Borchers, R. Kirchheim, Crack and blister initiation and growth in purified iron due to hydrogen loading, Acta Mater. 115 (2016) 24–34. doi:10.1016/j.actamat.2016.05.034.

[13] T.J. Marrow, M. Aindow, P. Prangnell, M. Strangwood, J.F. Knott, Hydrogen-assisted stable crack growth in iron-3 wt% silicon steel, Acta Mater. 44 (1996) 3125–3140. doi:10.1016/1359-6454(95)00429-7.

[14] F. Nakasato, I. Bernstein, Crystallographic and fractographic studies of hydrogen- induced cracking in purified iron and iron- silicon alloys, Metall. Mater. Trans. A. 9 (1978) 1317–1326. doi:10.1007/bf02652256.

[15] D. Birenis, Y. Ogawa, H. Matsunaga, O. Takakuwa, J. Yamabe, Ø. Prytz, et al., Hydrogen-assisted crack propagation in α-iron during elasto-plastic fracture toughness tests, Mater. Sci. Eng. A. 756 (2019) 396–404. doi:10.1016/j.msea.2019.04.084.

[16] X. Chen, W.W. Gerberich, The Kinetics and Micromechanics of Hydrogen- Assisted Cracking in Fe-3 Pct Si Single Crystals, Metall. Trans. A. 22 (1991) 59–70. doi:10.1007/BF03350949.

[17] O. Takakuwa, Y. Ogawa, S. Okazaki, M. Nakamura, H. Matsunaga, A mechanism behind hydrogen-assisted fatigue crack growth in ferrite-pearlite steel focusing on its behavior in gaseous environment at elevated temperature, Corros. Sci. 168 (2020). doi:10.1016/j.corsci.2020.108558.

[18] D. Birenis, Y. Ogawa, H. Matsunaga, O. Takakuwa, J. Yamabe, Ø. Prytz, et al., Interpretation of hydrogen-assisted fatigue crack propagation in BCC iron based on dislocation structure evolution around the crack wake, Acta Mater. 156 (2018) 245–253. doi:10.1016/j.actamat.2018.06.041.

[19] S.P. Lynch, Metallographic and fractographic techniques for characterising and understanding hydrogen-assisted cracking of metals, in: R.P. Gangloff, B.P. Somerday (Eds.), Gaseous Hydrog. Embrittlement Mater. Energy Technol. Vol. 1 Probl. Its Characterisation Eff. Part. Alloy Classes, Woodhead Publishing Limited, 2012: pp. 274–346. doi:10.1533/9780857093899.2.274.

[20] T. Neeraj, R. Srinivasan, J. Li, Hydrogen embrittlement of ferritic steels: Observations on

deformation microstructure, nanoscale dimples and failure by nanovoiding, Acta Mater. 60 (2012) 5160–5171. doi:http://dx.doi.org/10.1016/j.actamat.2012.06.014.

[21] S.P. Lynch, Environmentally assisted cracking: Overview of evidence for an adsorption-induced localised-slip process, Acta Metall. 36 (1988) 2639–2661. doi:10.1016/0001-6160(88)90113-7.

[22] S.P. Lynch, Hydrogen embrittlement phenomena and mechanisms, Corros. Rev. 30 (2012) 63–133. doi:10.1515/corrrev-2012-0502.

[23] I.M. Robertson, P. Sofronis, A. Nagao, M.L. Martin, S. Wang, D.W. Gross, et al., Hydrogen Embrittlement Understood, Metall. Mater. Trans. A. 46 (2015) 2323–2341. doi:10.1007/s11661-015-2836-1.

[24] M. Nagumo, Fundamentals of Hydrogen Embrittlement, Springer Singapore, Singapore, 2016. doi:10.1007/978-981-10-0161-1.

[25] M.L. Martin, M. Dadfarnia, A. Nagao, S. Wang, P. Sofronis, Enumeration of the hydrogen-enhanced localized plasticity mechanism for hydrogen embrittlement in structural materials, Acta Mater. 165 (2019) 734–750. doi:10.1016/j.actamat.2018.12.014.

[26] M. Djukic, G. Bakic, V. Sijacki Zeravcic, A. Sedmak, B. Rajicic, Hydrogen Embrittlement of Industrial Components: Prediction, Prevention and Models, Corrosion. (2016) 1958. doi:10.5006/1958.

[27] A.. Tetelman, W.. Robertson, Direct observation and analysis of crack propagation in iron-3% silicon single crystals, Acta Metall. 11 (1963) 415–426. doi:10.1016/0001-6160(63)90166-4.

[28] M. Gell, W.. Robertson, An analysis of plastic deformation around stationary cleavage cracks, Acta Metall. 14 (1966) 481–490. doi:10.1016/0001-6160(66)90316-6.

[29] H. Vehoff, W. Rothe, Gaseous hydrogen embrittlement in FeSi- and Ni-single crystals, Acta Metall. 31 (1983) 1781–1793. doi:10.1016/0001-6160(83)90125-6.

[30] Y. Takahashi, K. Yamaguchi, M. Tanaka, K. Higashida, H. Noguchi, On the micromechanism of hydrogen-assisted cracking in a single-crystalline iron-silicon alloy thin sheet, Scr. Mater. 64 (2011) 537–540. doi:10.1016/j.scriptamat.2010.11.035.

[31] Y. Takahashi, M. Tanaka, K. Higashida, K. Yamaguchi, H. Noguchi, An intrinsic effect of

hydrogen on cyclic slip deformation around a {1 1 0} fatigue crack in Fe-3.2 wt.% Si alloy, Acta Mater. 58 (2010) 1972–1981. doi:10.1016/j.actamat.2009.11.040.

[32] N. Takano, K. Kidani, Y. Hattori, F. Terasaki, Fracture surface of hydrogen embrittlement in iron single crystals, Scr. Metall. Mater. 29 (1993) 75–80. doi:10.1016/0956-716X(93)90257-S.

[33] S. Hinotani, Y. Ohmori, F. Terasaki, Hydrogen crack initiation and propagation in pure iron single crystal, Mater. Sci. Technol. (United Kingdom). 10 (1994) 141–148. doi:10.1179/mst.1994.10.2.141.

[34] Y. Ogawa, D. Birenis, H. Matsunaga, A. Thøgersen, Ø. Prytz, O. Takakuwa, et al., Multi-scale observation of hydrogen-induced, localized plastic deformation in fatigue-crack propagation in a pure iron, Scr. Mater. 140 (2017) 13–17. doi:10.1016/j.scriptamat.2017.06.037.

[35] Y. Takahashi, H. Nishikawa, Y. Oda, H. Noguchi, Microscopic characterization of hydrogen-induced quasi-brittle fatigue fracture in low-strength carbon steel, Mater. Lett. 64 (2010) 2416–2419. doi:10.1016/j.matlet.2010.08.019.

[36] K. Okada, A. Shibata, Y. Takeda, N. Tsuji, Crystallographic feature of hydrogen-related fracture in 2Mn-0.1C ferritic steel, Int. J. Hydrogen Energy. 43 (2018) 11298–11306. doi:10.1016/j.ijhydene.2018.05.011.

[37] T. Homma, S. Anata, S. Onuki, K. Takai, Crack initiation and propagation behavior of hydrogen-induced quasi-cleavage fracture in X80 pipeline steel with stress concentration, Tetsu-To-Hagane/Journal Iron Steel Inst. Japan. 106 (2020) 651–661. doi:10.2355/tetsutohagane.TETSU-2019-126.

[38] E.D. Merson, V.A. Poluyanov, P.N. Myagkikh, D.L. Merson, A. Vinogradov, Quantitative comparison of cleavage and quasi-cleavage fracture surfaces in hydrogen embrittled low-carbon steel, Lett. Mater. 10 (2020) 303–308.

[39] E. Merson, V. Danilov, D. Merson, A. Vinogradov, Confocal laser scanning microscopy: The technique for quantitative fractographic analysis, Eng. Fract. Mech. 183 (2017) 147–158. doi:10.1016/j.engfracmech.2017.04.026.

[40] E. Merson, A.V. Kudrya, V.A. Trachenko, D. Merson, V. Danilov, A. Vinogradov, The Use of Confocal Laser Scanning Microscopy for the 3D Quantitative Characterization of

Fracture Surfaces and Cleavage Facets, Procedia Struct. Integr. 2 (2016) 533–540. doi:10.1016/j.prostr.2016.z06.069.

[41] E. Merson, A.V. Kudrya, V.A. Trachenko, D. Merson, V. Danilov, A. Vinogradov, Quantitative characterization of cleavage and hydrogen-assisted quasi-cleavage fracture surfaces with the use of confocal laser scanning microscopy, Mater. Sci. Eng. A. 665 (2016) 35–46. doi:10.1016/j.msea.2016.04.023.

[42] E.D. Merson, V.A. Poluyanov, D.L. Merson, A.Y. Vinogradov, About the Nature of Quasi-Cleavage in Low-Carbon Steel Embrittled with Hydrogen, Met. Sci. Heat Treat. 61 (2019) 191–195. doi:10.1007/s11041-019-00399-x.

[43] E.D. Merson, P.N. Myagkikh, V.A. Poluyanov, D.L. Merson, A. Vinogradov, Quasi-cleavage hydrogen-assisted cracking path investigation by fractographic and side surface observations, Eng. Fract. Mech. 214 (2019) 177–193. doi:10.1016/j.engfracmech.2019.04.042.

[44] A. Laureys, T. Depover, R. Petrov, K. Verbeken, Influence of sample geometry and microstructure on the hydrogen induced cracking characteristics under uniaxial load, Mater. Sci. Eng. A. 690 (2017) 88–95. doi:10.1016/j.msea.2017.02.094.